



TVD differencing on three-dimensional unstructured meshes with monotonicity-preserving correction of mesh skewness



Fabian Denner*, Berend G.M. van Wachem

Thermofluids Division, Department of Mechanical Engineering, Imperial College London, Exhibition Road, London, SW7 2AZ, United Kingdom

ARTICLE INFO

Article history:

Received 17 April 2015

Accepted 12 June 2015

Available online 19 June 2015

Keywords:

TVD schemes

Hyperbolic partial differential equations

Monotonicity

Mesh skewness

Unstructured meshes

ABSTRACT

Total variation diminishing (TVD) schemes are a widely applied group of monotonicity-preserving advection differencing schemes for partial differential equations in numerical heat transfer and computational fluid dynamics. These schemes are typically designed for one-dimensional problems or multidimensional problems on structured equidistant quadrilateral meshes. Practical applications, however, often involve complex geometries that cannot be represented by Cartesian meshes and, therefore, necessitate the application of unstructured meshes, which require a more sophisticated discretisation to account for their additional topological complexity. In principle, TVD schemes are applicable to unstructured meshes, however, not all the data required for TVD differencing is readily available on unstructured meshes, and the solution suffers from considerable numerical diffusion as a result of mesh skewness. In this article we analyse TVD differencing on unstructured three-dimensional meshes, focusing on the non-linearity of TVD differencing and the extrapolation of the virtual upwind node. Furthermore, we propose a novel monotonicity-preserving correction method for TVD schemes that significantly reduces numerical diffusion caused by mesh skewness. The presented numerical experiments demonstrate the importance of accounting for the non-linearity introduced by TVD differencing and of imposing carefully chosen limits on the extrapolated virtual upwind node, as well as the efficacy of the proposed method to correct mesh skewness.

© 2015 The Authors. Published by Elsevier Inc. This is an open access article under the CC BY license (<http://creativecommons.org/licenses/by/4.0/>).

1. Introduction

The discretisation of spatial advection terms is at the heart of numerical heat and mass transfer as well as computational fluid dynamics (CFD) and is extensively discussed in the literature, e.g. [1–3]. Differencing schemes suitable for the discretisation of spatial advection terms should be robust, high-order accurate and monotonicity-preserving. However, high-order differencing schemes can cause oscillations in the solution, thus, violating monotonicity [4]. *Total variation diminishing* (TVD) schemes, based on the seminal work of Harten [5] and Sweby [6], denote a group of differencing schemes particularly designed to preserve an oscillation-free solution. TVD schemes, able to achieve a stable high-order discretisation while satisfying the monotonicity criterion [5], have been widely adopted since their introduction and represent the *de facto* standard for the discretisation of advection terms in finite difference and finite volume methods. Historically, most TVD schemes have been derived and tested with one-dimensional test-cases on equidistant meshes. This is a simplification of the multi-dimensional applications typically found in heat and mass transfer as well as fluid dynamics. Furthermore, the non-linearity

* Corresponding author. Tel.: +44 7500 060 053.

E-mail address: fabian.denner@gmail.com (F. Denner).

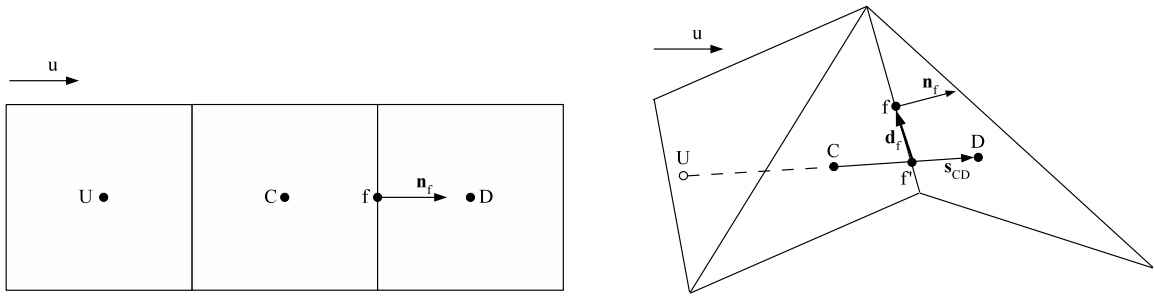


Fig. 1. Example of the upwind U , central C and downwind D nodes with respect to face f on a structured mesh (left) and an unstructured mesh (right), including relevant interpolation entities.

inherently introduced by TVD differencing [7], since the choice of differencing scheme is dependent on the advected scalar field, is a frequently overlooked issue in the relevant literature, even though oscillations caused by compressive TVD schemes reported in previous studies [8–11] may be attributed to this non-linearity.

Although the implementation of TVD schemes on multidimensional Cartesian meshes with structured, equidistant cell arrangement is straightforward, the implementation of such schemes on unstructured meshes comprises additional difficulties as a result of the additional topological complexity and the resulting skewness of such meshes. The most frequently cited problem in the literature is the determination of the upwind node necessary for a TVD formulation, which is not readily available on unstructured meshes, as shown in Fig. 1. Ubbink and Issa [12] as well as Darwish and Moukalled [13] derived second-order accurate approximations of the value at the upwind node, using data readily available on unstructured meshes. Although both approximations are founded on the same basic principles, Ubbink and Issa [12] calculate the value at a virtual upwind node explicitly, whereas Darwish and Moukalled [13] proposed to account for the value at the upwind node in an implicit fashion. Both approximations reconstruct the upwind value exactly on one-dimensional, equidistant meshes, yet this reconstruction becomes unreliable and possibly erroneous on non-equidistant meshes and non-rectilinear meshes. Other methods to extrapolate the upwind node on unstructured meshes, albeit less frequently encountered in the literature, have been proposed by Jasak et al. [14], Li et al. [8] and Zhang et al. [15]. Another common problem with the application of unstructured meshes is that the cells are typically not arranged equidistant to each other, which requires special care when face values are interpolated from values at adjacent cell centres. Hou et al. [9] have recently proposed the first consistent TVD formulation for non-equidistant meshes, significantly improving the accuracy of the interpolation on such meshes.

If the interpolation point associated with a mesh face, denoted as f' in Fig. 1, does not coincide with the geometrical centre of that face, commonly referred to as *mesh skewness* [16–18] and schematically illustrated on the right of Fig. 1, a diffusion-like error is introduced in the solution [16]. Although considerable mesh skewness is frequently encountered in unstructured meshes and has long been recognised as a problem in the relevant literature [16–21], the interpolation error introduced by mesh skewness as well as methods to mitigate this error have not been the focus of published research in the context of TVD schemes, despite the extensive research efforts dedicated to high-order differencing schemes. Denner and van Wachem [21] recently proposed a method to correct the error resulting from mesh skewness for donor–acceptor advection schemes designed to advect sharp interfaces, changing the implicit matrix coefficients of the linear system of equations to correct errors resulting from mesh skewness. This correction method successfully diminishes numerical diffusion due to mesh skewness and retains the conservation and monotonicity-preserving characteristics of the underlying interface advection schemes. TVD schemes and donor–acceptor schemes follow a similar basic approach, as both compute a weighting factor, typically called *flux limiter*, of upwind and downwind values for a given mesh face. While donor–acceptor schemes for the advection of sharp interfaces, such as CICSAM [12] or STACS [22], determine the flux limiter based on the orientation of the interface, TVD schemes determine the flux limiter based on the ratio of upwind to downwind gradients of the advected scalar.

In this article we scrutinise the accuracy and application of TVD differencing schemes on unstructured meshes, especially focusing on problems resulting from the non-linearity introduced by TVD differencing and the extrapolation of the virtual upwind node. Furthermore, we propose a novel method for TVD schemes to correct the error due to mesh skewness that retains the monotonicity-preserving properties of TVD schemes and only requires data readily available on unstructured meshes, based on the principles introduced by Denner and van Wachem [21]. Particular attention is given to the limits explicitly imposed on the skewness-corrected flux limiter.

The article is structured as follows. In Section 2 the numerical framework is outlined and, in Section 3, the implementation of TVD differencing on unstructured meshes is discussed. Subsequently, Section 4 is concerned with numerical diffusion caused by mesh skewness and introduces a new method to correct the error due mesh skewness for TVD schemes. The results of numerical experiments using three representative test-cases are presented and discussed in Section 5. The findings are summarised and the article is concluded in Section 6.

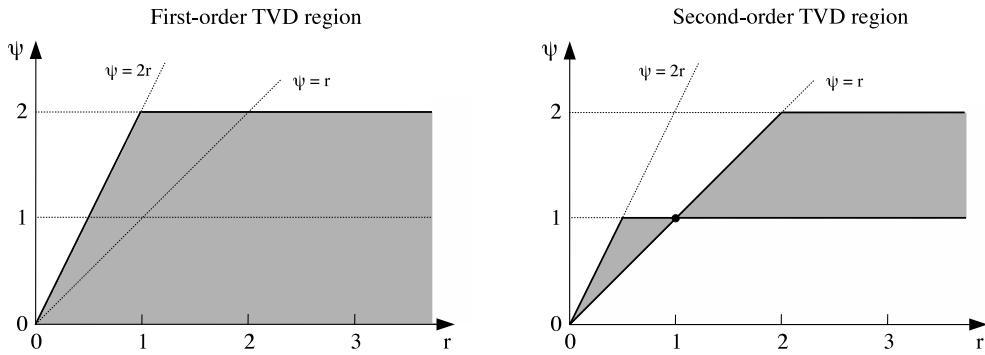


Fig. 2. Flux limiter ψ as a function of the gradient ratio r with the first-order TVD region (left) and the second-order TVD region (right) shaded in grey [6].

2. Numerical framework

The linear advection equation for a general fluid variable ϕ is given as

$$\frac{\partial \phi}{\partial t} + u_i \frac{\partial \phi}{\partial x_i} = 0, \tag{1}$$

where t is time, \mathbf{x} is the spatial coordinate and \mathbf{u} is the velocity vector. To numerically compute a solution, Eq. (1) is discretised in the present study using the finite volume method. For a given mesh cell C , illustrated in Fig. 1, the transient term of Eq. (1) is discretised using the Second-Order Backward Euler scheme [1],

$$\int_{V_C} \frac{\partial \phi}{\partial t} dV \approx \frac{3\phi_C^t - 4\phi_C^{t-\Delta t} + \phi_C^{t-2\Delta t}}{2\Delta t} V_C, \tag{2}$$

where Δt is the applied time-step, V_C is the volume of cell C and the superscripts of ϕ denote the time level. The spatial advection term of ϕ in Eq. (1) is discretised by integration over the cell volume using the divergence theorem and the midpoint rule, following as

$$\int_{V_C} u_i \frac{\partial \phi}{\partial x_i} dV \approx \sum_f \phi_f (\mathbf{u}_f \cdot \mathbf{n}_f) A_f, \tag{3}$$

where f are the mesh faces bounding mesh cell C , ϕ_f is the fluid variable at the centre of face f , \mathbf{n}_f is the outward-pointing normal vector of face f and A_f is the area of face f . The fluid variable ϕ_f at face f is evaluated using a suitable differencing scheme, further discussed in Section 3. The discretised advection equation, Eq. (1), is implemented implicitly and the resulting system of linear equations, $\mathbf{A} \cdot \mathbf{x} = \mathbf{b}$, is solved using a conjugated-gradient solver incorporated in the freely-available software library PETSc [23,24]. Although the advection equation given in Eq. (1) is linear, the TVD flux limiter introduces non-linearity because it is dependent on the distribution of scalar ϕ , as further explained in Section 5.3. In order to account for the resulting non-linearity of the discretised advection equation, each time-step consists of a finite number of non-linear iterations (*inexact Newton method* [25]).

3. TVD differencing

Using a TVD scheme to determine face value ϕ_f in Eq. (3) based on the adjacent cell values ϕ_C and ϕ_D , see Fig. 1, face value ϕ_f is given as [3]

$$\phi_f = \phi_C + \frac{\psi(r_f)}{2} (\phi_D - \phi_C) = \left[1 - \frac{\psi(r_f)}{2} \right] \phi_C + \frac{\psi(r_f)}{2} \phi_D, \tag{4}$$

where $\psi(r_f)$ represents the flux limiter. TVD schemes are designed to achieve a monotonicity preserving, high-order discretisation. In order for a scheme to preserve the monotonicity of the solution, local minima must be non-decreasing, local maxima must be non-increasing and the discretisation must not create new local extrema. TVD schemes are by default monotonicity-preserving, as they require the total variation of a solution to be non-increasing [5],

$$\sum_{P=1}^N \nabla \phi_P^{t+\Delta t} V_P \leq \sum_{P=1}^N \nabla \phi_P^t V_P, \tag{5}$$

with N being the total number of mesh cells. For a differencing scheme to be TVD, Sweby [6] derived the following conditions of the flux limiter ψ as a function of the local gradient ratio r_f , illustrated in the left graph of Fig. 2:

- $\psi(r_f) = 0$ for $r_f \leq 0$,
- $0 \leq \psi(r_f) \leq 2r_f$ for $0 < r_f < 1$, and
- $0 \leq \psi(r_f) \leq 2$ for $r_f \geq 1$.

The gradient ratio r_f of ϕ at face f is defined as

$$r_f = \frac{\phi_C - \phi_U}{\phi_D - \phi_C}, \tag{6}$$

where subscripts C , D and U denote the central, downwind and upwind nodes, respectively, with regards to face f , illustrated in Fig. 1. Differencing schemes that satisfy these conditions are TVD and of minimum first-order accuracy. The flux limiter of a second-order TVD scheme must lie within the more restrictive parameter space depicted in grey in the right graph of Fig. 2. Furthermore, the function to determine the flux limiter should be symmetric, i.e. backward-facing and forward-facing gradients are treated in the same manner.

3.1. Inverse-distance weighting

The interpolation of ϕ_f in Eq. (4) is based on the assumption that face f is situated at equal distances from nodes C and D . However, unstructured three-dimensional meshes are in general not equidistant, compromising the accuracy of ϕ_f calculated based on Eq. (4). On a non-equidistant mesh a second-order accurate spatial interpolation of the face value is achieved by applying an inverse-distance weighting of the adjacent cell-centred values [26]. Hou et al. [9] derived a complete formulation for TVD differencing based on inverse-distance weighting, in which face value ϕ_f is calculated as

$$\phi_f = \left[1 - \frac{\psi(r_f)}{L} \right] \phi_C + \frac{\psi(r_f)}{L} \phi_D, \tag{7}$$

with

$$L = \frac{|\mathbf{s}_{Cf}| + |\mathbf{s}_{Df}|}{|\mathbf{s}_{Cf}|}, \tag{8}$$

where \mathbf{s}_{Cf} is the vector from node C to face f and \mathbf{s}_{Df} is the vector from node D to face f . For a consistent TVD formulation this weighting also has to be applied to the definition of the flux limiter $\psi(r_f)$. The first-order TVD region changes from $0 \leq \psi(r_f) \leq \max(0, \min(2r_f, 2))$ for equidistant meshes to $0 \leq \psi(r_f) \leq \max(0, \min(Lr_f, L))$ for non-equidistant meshes [9]. The revised TVD region, including the second-order TVD limits, for non-equidistant meshes is shown in Fig. 3, following the work of Hou et al. [9].

3.2. Upwind value on unstructured meshes

As illustrated in Fig. 1, the upwind node U is not readily available on arbitrary, unstructured meshes and has to be approximated by a suitable method. Darwish and Moukalled [13] devised a formally second-order accurate formulation of the gradient ratio r_f , defined as

$$r_f = \frac{2 \nabla \phi|_C \cdot \mathbf{s}_{CD} - (\phi_D - \phi_C)}{\phi_D - \phi_C} = \frac{2 \nabla \phi|_C \cdot \mathbf{s}_{CD}}{\phi_D - \phi_C} - 1, \tag{9}$$

placing the upwind node U along the line joining nodes C and D , with nodes U and D positioned equidistant to node C . The vector \mathbf{s}_{CD} is the vector connecting cell centres C and D , as depicted in Fig. 1. All the data required to determine r_f from Eq. (9) is readily available on unstructured meshes and on equidistant Cartesian meshes this formulation reverts to the exact gradient ratio as defined in Eq. (6).

An alternative formulation of gradient ratio r_f on unstructured meshes can be devised based on

$$r_f = \frac{\phi_C - \phi_U^*}{\phi_D - \phi_C}, \tag{10}$$

where ϕ_U^* is the value at the virtual upwind node. Following the work of Ubbink and Issa [12], this virtual upwind value is explicitly extrapolated as

$$\phi_U^* = \phi_D - 2 \nabla \phi_f \mathbf{s}_{CD}. \tag{11}$$

This extrapolation of the upwind value has also been used by Darwish and Moukalled [13] in their derivation of Eq. (9). However, calculating ϕ_U^* explicitly provides the opportunity to bound the value at the upwind node with appropriate limits, as suggested by Ubbink and Issa [12], for instance using the minimum and maximum value in the immediate neighbourhood of node U^* .

Li et al. [8] erroneously state that Eq. (9) misrepresents the gradient ratio if the variation in ϕ is exponential. Using a basic finite difference (or finite volume) discretisation on an equidistant, one-dimensional mesh with an exponential

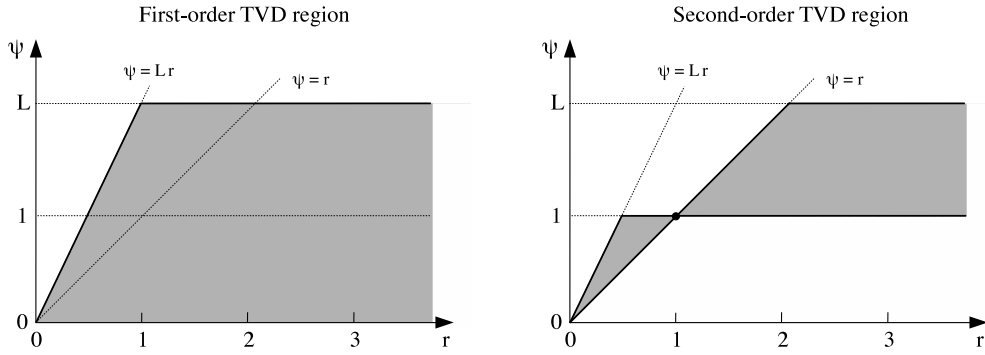


Fig. 3. Flux limiter ψ as a function of the gradient ratio r with the first-order TVD region (left) and the second-order TVD region (right) shaded in grey for a non-equidistant mesh [9].

variation of ϕ , as depicted on the left of Fig. 4, the resulting gradient ratio $r_f = 0.01$ is correctly represented by Eq. (9) as well as Eq. (10). If, however, the face is not situated halfway between the adjacent cell centres but, for instance, moved toward the downwind cell D , illustrated on the right of Fig. 4, the gradient of ϕ is overestimated and the resulting gradient ratio $r_f = 0.34$ given by Eq. (9) is not exact anymore and, in this particular case, results in a more compressive differencing scheme. In general, this misinterpretation of the gradient ratio may cause the flux limiter to lie outside the TVD region of the actual gradient ratio of the solution, potentially violating monotonicity [7]. However, using the extrapolation method of Ubbink and Issa [12], see Eq. (11), and simply bounding ϕ_U^* by the lower limit $\phi^- = 0$, Eq. (10) approximates the gradient ratio $r_f = 0.0101$ with sufficient accuracy. An accurately bounded upwind value is essential on three-dimensional unstructured meshes as further demonstrated in Section 5.4.

3.3. Differencing schemes

A considerable number of first- and second-order TVD schemes have been published in the literature, e.g. [6,27–30]. For most general problems, the solution provided by these schemes is very similar and major differences are only noticeable for extreme cases, such as shocks or phase boundaries. Three representative second-order TVD differencing schemes, illustrated in Fig. 5 in the modified r - ψ diagram of Sweby [6], are considered as part of this study:

1. the MINMOD scheme [29] with $\psi(r_f) = \max(0, \min(1, r_f))$,
2. the van Leer scheme [27] with $\psi(r_f) = (0.5 L r_f + 0.5 L |r_f|) / (L - 1 + |r_f|)$, and
3. the SUPERBEE scheme [29] with $\psi(r_f) = \max(0, \min(1, L r_f), \min(r_f, L))$.

The van Leer and SUPERBEE schemes, as given above, are reformulated for non-equidistant meshes as proposed by Hou et al. [9]. The original form of these schemes is retained with $L = 2$, i.e. for an equidistant mesh. The MINMOD scheme follows the diffusive boundary of the second-order TVD region, as seen in Fig. 5, and, thus, represents the most diffusive second-order TVD schemes. The SUPERBEE scheme, on the other hand, follows the compressive boundary of the second-order TVD region, constituting the most compressive second-order TVD scheme. The van Leer scheme varies smoothly in the second-order TVD region of the r - ψ diagram. All three TVD schemes revert to a first-order upwind scheme ($\psi(r_f) = 0$) for $r_f \leq 0$, which is a necessary condition for TVD schemes [28].

4. Correction of mesh skewness

Skewness is a common issue on non-Cartesian, arbitrary meshes. As a result of skewness, the geometric face centre f does not coincide with the interpolation point f' of this face, as depicted on the right of Fig. 1. Thus, the linearly interpolated face value becomes inaccurate and the accuracy of the interpolation reduces formally to first order [1]. As shown by Jasak [16], mesh skewness causes a diffusion-like discretisation error E_s , similar to the leading truncation error of the first-order upwind scheme, given for cell C as

$$E_{s,C} = \sum_f (\mathbf{d}_f \cdot \nabla \phi|_f) \mathbf{u}_f \mathbf{n}_f A_f, \tag{12}$$

where \mathbf{d}_f is the vector from interpolation point f' to face centre f , as shown on the right of Fig. 1. Following Jasak [16], the error induced by mesh skewness can be formulated as the diffusion term

$$E_s = \frac{\partial}{\partial x_i} \left(\Gamma_s \frac{\partial \phi}{\partial x_i} \right), \tag{13}$$

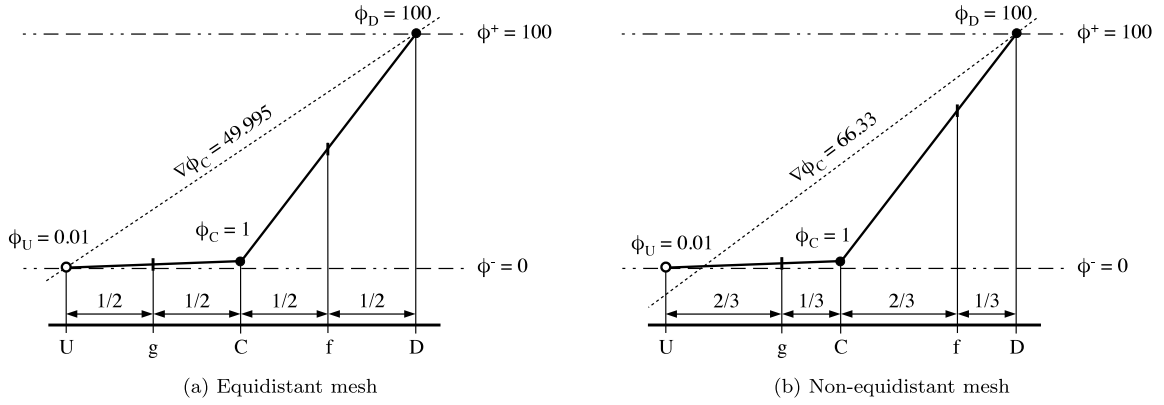


Fig. 4. One-dimensional example of exponential growth of scalar ϕ , including the mesh entities associated with a TVD discretisation and extrapolation of the upwind node, on an equidistant mesh (left) and a non-equidistant mesh (right). ϕ^- and ϕ^+ are the theoretical minimum and maximum values of ϕ , respectively.

where $\Gamma_s = \mathbf{u}_f \cdot \mathbf{d}_f$ is the diffusion coefficient due to mesh skewness. Thus, Eq. (1) becomes [21]

$$\frac{\partial \phi}{\partial t} + u_i \frac{\partial \phi}{\partial x_i} = - \frac{\partial}{\partial x_i} \left(\Gamma_s \frac{\partial \phi}{\partial x_i} \right). \tag{14}$$

Hence, interpolating cell-centred values to face centres without correcting the error resulting from mesh skewness, as for instance by means of Eq. (7), leads to significant numerical diffusion on meshes with appreciable skewness. The explicit correction of mesh skewness, with the advected scalar corrected for skewness $\hat{\phi}_f$ at face f given as

$$\hat{\phi}_f = \phi_f + \nabla \phi|_f \cdot \mathbf{d}_f, \tag{15}$$

is widely applied to reduce the absolute error of the solution and to raise the formal accuracy of spatial interpolation on unstructured meshes to second order [16–20,31]. However, this explicit skewness correction may violate the monotonicity of the resulting face value ϕ_f and may adversely affect the stability of the solving algorithm on meshes with high mesh skewness or in regions with large gradients of ϕ [21].

4.1. Skewness-corrected flux limiter

In order to account for the numerical diffusion induced by mesh skewness, a correction of the flux limiter is proposed, following the work of Denner and van Wachem [21] for interface advection schemes. Based on the definition of the face value presented in Eq. (7), Eq. (15) can be formulated as [21]

$$\hat{\phi}_f = \left[1 - \frac{\psi(r_f)}{L} \right] \phi_C + \frac{\psi(r_f)}{L} \phi_D + \nabla \phi|_f \cdot \mathbf{d}_f \tag{16}$$

or, alternatively,

$$\hat{\phi}_f = \left[1 - \frac{\hat{\psi}(r_f)}{L} \right] \phi_C + \frac{\hat{\psi}(r_f)}{L} \phi_D, \tag{17}$$

where $\hat{\psi}(r_f)$ is the skewness-corrected flux limiter. Inserting Eq. (16) in Eq. (17) and rearranging for $\hat{\psi}(r_f)$, the skewness-corrected flux limiter follows as

$$\hat{\psi}(r_f) = \psi(r_f) + \frac{L \nabla \phi|_f \cdot \mathbf{d}_f}{\phi_D - \phi_C}. \tag{18}$$

The skewness-corrected flux limiter $\hat{\psi}(r_f)$ corrects the face value of ϕ implicitly if skewness is present, taking into account the value of ϕ at the adjacent cells as well as the magnitude and the direction of the skewness error E_s .

4.2. Enforcing TVD limits

It is essential that the skewness-corrected flux limiter $\hat{\psi}(r_f)$ is carefully bounded to satisfy the TVD condition, Eq. (5), and preserves the monotonicity of the solution. Bounding the flux limiter by

$$0 \leq \hat{\psi}(r_f) \leq \max(0, \min(L r_f, L)) \tag{19}$$

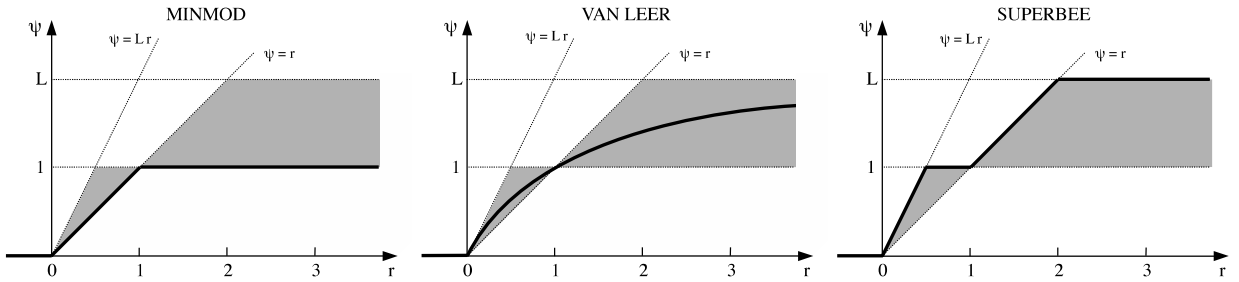


Fig. 5. Flux limiter ψ as a function of the gradient ratio r for three representative TVD schemes used in this study. The shaded area represents the second-order TVD region [9].

assures a bounded solution of first-order accuracy, depicted by the shaded area in the graph on the left of Fig. 3, and bounding the flux limiter by

$$\max(0, \min(r_f, 1)) \leq \hat{\psi}(r_f) \leq \max(0, \min(Lr_f, 1), \min(r_f, L)), \quad (20)$$

as illustrated in the graph on the right of Fig. 3, leads to a bounded solution with formal second-order accuracy. The first-order limits (FOL) defined in Eq. (19) give the skewness correction a wider range to adapt the flux limiter and counteract numerical diffusion induced by mesh skewness, which is generally preferable on meshes with significant skewness. Furthermore, FOL do not affect the formal order of accuracy, since mesh skewness reduces the formal order of accuracy of the interpolation to first order anyway [1]. The second-order limits (SOL) defined in Eq. (20), on the other hand, retain a high-order accuracy for meshes with moderate skewness. It is not possible to make an *a priori* statement whether FOL or SOL should be applied, as the efficacy of the skewness correction and its limits is dependent on the advected scalar field and the mesh quality. Applying the revised flux limiter $\hat{\psi}(r_f)$ instead of $\psi(r_f)$ in Eq. (4) is expected to significantly reduce numerical diffusion as a result of mesh skewness.

5. Results

The test-cases used in this study are introduced and the initial conditions are described in Section 5.1. Section 5.2 scrutinises the overall performance of the considered TVD schemes on equidistant Cartesian and tetrahedral meshes, followed by a study of the effect of non-linearity on the TVD properties in Section 5.3. Section 5.4 investigates and discusses the implications associated with the two methods of upwind node extrapolation described in Section 3.2. The proposed method to correct the error resulting from mesh skewness is examined in Section 5.5.

5.1. Test-cases

The results for three pure-advection cases, illustrated in Fig. 6, are presented to validate and scrutinise the presented TVD formulations and the proposed monotonicity-preserving correction of mesh skewness.

A test-case frequently used in similar form to test and validate advection schemes, see e.g. [3,8,9,13,16], is the advection of a step profile oriented tangential to the flow, hereafter called *tangential step advection*, shown in Fig. 6(a). The computational domain used in this study has the dimensions $1 \text{ m} \times 1 \text{ m} \times 0.1 \text{ m}$ and is represented by 38,768 tetrahedral mesh cells. An equidistant Cartesian mesh with 200×200 cells is used as a reference. The step profile is advected with $u = 1 \text{ m s}^{-1}$ at an angle of 50° to the x -axis. The applied time-step represents a Courant number of $Co = u \Delta t / \Delta x = 0.5$ and the simulation is run until the steady-state solution is fully developed.

The advection of a sinusoidal profile and a double-step profile oriented perpendicular to the flow, henceforth referred to as *normal wave advection* and *normal step advection*, respectively, is illustrated in Figs. 6(b) and 6(c). The computational domain for these normal advection cases has the dimensions $2 \text{ m} \times 1 \text{ m} \times 0.05 \text{ m}$ and is represented by 408,585 tetrahedral mesh cells. Reference results are obtained on a two-dimensional equidistant Cartesian mesh with 500×250 cells. The scalar field is advected in positive x -direction at a constant velocity of $u = 1 \text{ m s}^{-1}$ and the applied time-step corresponds to $Co = 0.3$. The sinusoidal profile of the normal wave advection is initialised as $\phi = 0$ for $x \leq 0.1 \text{ m}$, $\phi = 0.5 - 0.5 \cos\{\pi(x - 0.1 \text{ m})/0.3 \text{ m}\}$ for $0.1 \text{ m} < x < 0.4 \text{ m}$ and $\phi = 1$ for $x \geq 0.4 \text{ m}$. The discontinuities in ϕ of the normal step advection are initially positioned at $x = 0.2 \text{ m}$ and $x = 0.3 \text{ m}$.

5.2. General performance

The considered TVD schemes, discussed in Section 3.3, are examined using the three representative test-cases to gain a better understanding of the performance of the individual schemes on structured and unstructured meshes. Solutions obtained with the first-order upwind differencing scheme, $\psi(r_f) = 0$, are also shown as a reference.

Fig. 7 shows the steady-state result of the tangential step advection along the x -axis at $y = 0.9 \text{ m}$, on the equidistant Cartesian mesh and the tetrahedral mesh. Of the three tested TVD schemes, the MINMOD scheme results in the most

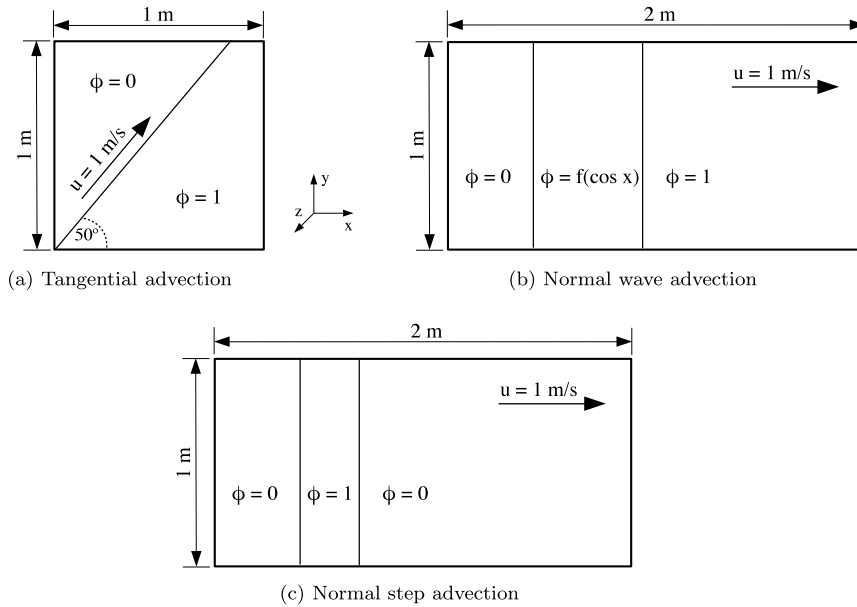


Fig. 6. Schematic illustration of the three considered pure-advection cases.

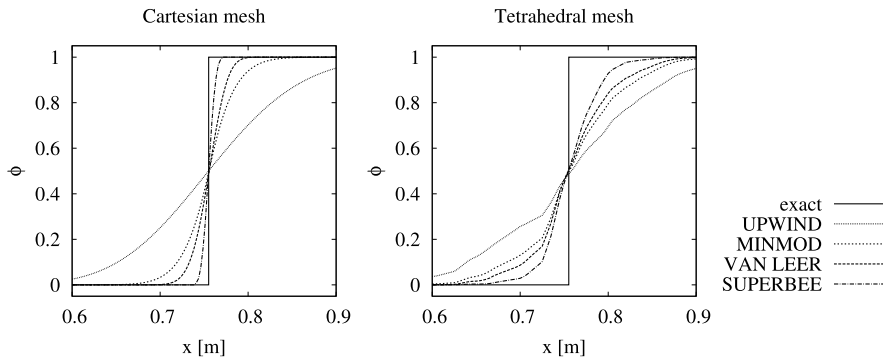


Fig. 7. Profile of ϕ along the x -axis at $y = 0.9 \text{ m}$ of the tangential step advection on the equidistant Cartesian mesh (left) and the tetrahedral mesh (right), comparing the considered TVD schemes.

diffusive profile, whereas the SUPERBEE scheme conserves the shape of the step profile most closely. All three TVD schemes result in a considerably more diffusive profile on the tetrahedral mesh compared to the results obtained on the Cartesian mesh. The results of the normal wave advection on both mesh types at $t = 1.5 \text{ s}$ are shown in Fig. 8. On the Cartesian mesh, the three TVD schemes represent the wave very accurately and perform similarly well. Upon close inspection of Fig. 8, a small deviation from the wave profile can be observed for the SUPERBEE scheme, which is the result of the compressive bias of the SUPERBEE scheme steepening the wave profile. The wave profile is also fairly well represented by the TVD schemes on the tetrahedral mesh, again with the MINMOD scheme resulting in the most diffusive profile among the TVD schemes. For the normal step advection, shown in Fig. 9, the performance of the TVD schemes on the Cartesian mesh are similar to the previously discussed cases, with SUPERBEE, van Leer and MINMOD ranking in increasing order of diffusiveness. However, the clear distinction between these schemes observed on the Cartesian mesh is diminished on the tetrahedral mesh, where in particular the performance of the van Leer and the SUPERBEE schemes becomes similarly diffusive.

As expected, the upwind scheme is the most diffusive of the tested schemes for all three cases and on both types of meshes, although the performance is fairly independent of the mesh type and the difference between TVD schemes and upwind scheme is significantly smaller on the tetrahedral meshes than on the Cartesian meshes.

5.3. Non-linearity

As mentioned in the introduction of this article, since the flux limiter $\psi(r_f)$ is a function of the solution itself, TVD differencing introduces non-linearity even if a linear transport equation is solved. This is an often overlooked property of

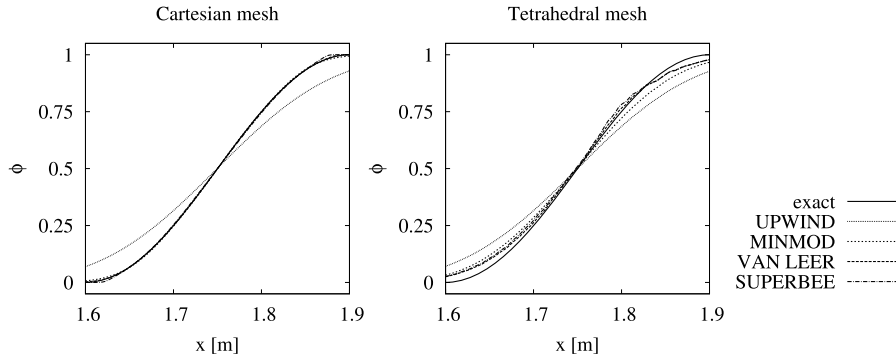


Fig. 8. Profile of ϕ along the x -axis at $t = 1.5$ s of the normal wave advection on the equidistant Cartesian mesh (left) and the tetrahedral mesh (right), comparing the considered TVD schemes.

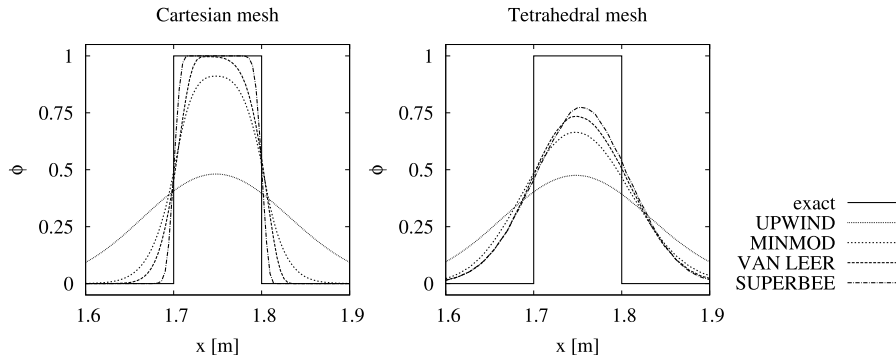


Fig. 9. Profile of ϕ along the x -axis at $t = 1.5$ s of the normal step advection on the equidistant Cartesian mesh (left) and the tetrahedral mesh (right), comparing the considered TVD schemes.

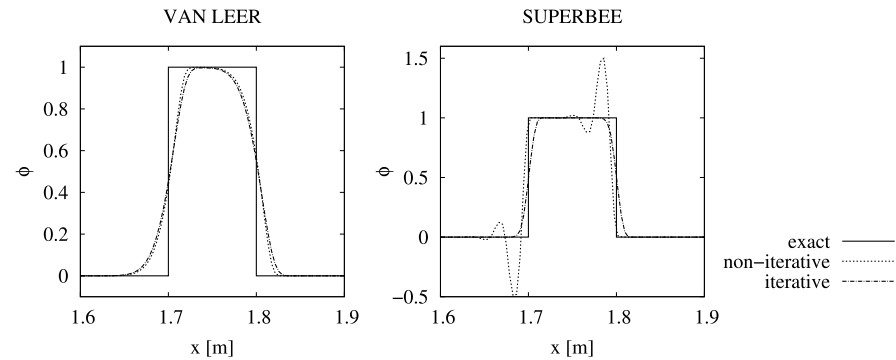


Fig. 10. Comparison of the solution along the x -axis obtained with a non-iterative and an iterative solution approach for the normal step advection after $t = 1.5$ s on the equidistant Cartesian mesh with 500×250 cells, using the van Leer (left) and the SUPERBEE (right) schemes.

TVD schemes with potentially profound implications. Deferring the evaluation of the flux limiter and solving the governing equation, Eq. (1), iteratively, as described in Section 2, is a readily available way to account for this non-linearity.

The graph on the left of Fig. 10 shows the distribution of ϕ along the x -axis of the normal step advection after $t = 1.5$ s using the van Leer scheme on the equidistant Cartesian mesh. The discrepancy introduced by the non-linearity of the flux limiter causes the scheme to be more compressive. Although in this particular case the van Leer scheme still preserves monotonicity even without accounting for the non-linearity of the flux limiter, this increase in compressiveness becomes problematic if the SUPERBEE scheme is applied, as seen in the graph on the right of Fig. 10. The non-iterative solution of Eq. (1) develops severe oscillations on the upwind-side of the discontinuities, whereas the iterative algorithm preserves the monotonicity of the solution. Such oscillations have been reported, without a comprehensive explanation, in a number of studies using the SUPERBEE scheme [8–11]. Examining the flux limiter of the SUPERBEE scheme in the Sweby diagram, see Fig. 5(d), it is clear that for $r_f < 1/L$ even a small error in the evaluation of r_f can mean the flux limiter $\psi(r_f)$ lies outside the TVD region with respect to the actual gradient ratio of the solution and is, therefore, no longer monotonicity-preserving.

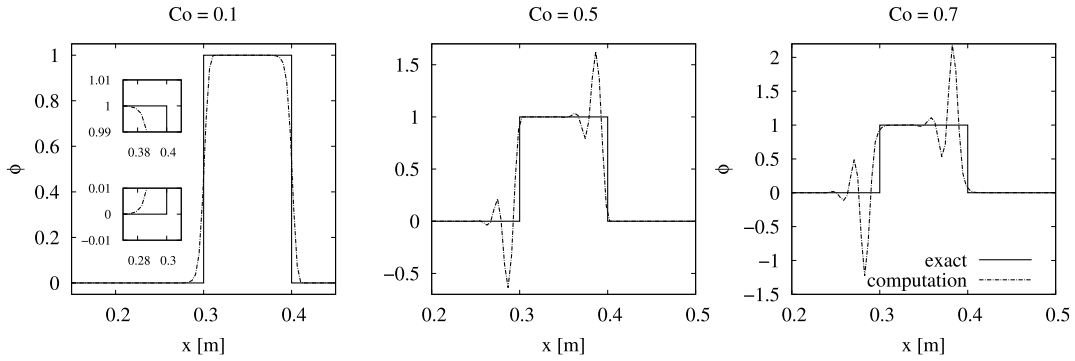


Fig. 11. Comparison of the solution along the x -axis obtained with a non-iterative solution approach for the normal step advection after $t = 0.1$ s on the equidistant Cartesian mesh with 500×250 cells using the SUPERBEE schemes with different Courant numbers.

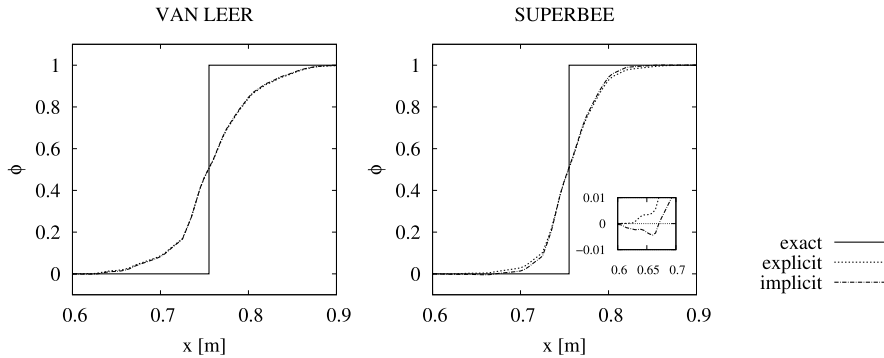


Fig. 12. Profile of ϕ along the x -axis at $y = 0.9$ m of the tangential step advection on the tetrahedral mesh at $y = 0.9$ m using the implicit upwind extrapolation of Darwish and Moukalled [13].

For the results presented in Fig. 10, the iterative algorithm requires a maximum of three non-linear iterations for the non-linear solution to converge.

Changing the time-step applied to solve the transient evolution of the scalar field and, hence, changing the Courant number $Co = u\Delta t/\Delta x$, the impact of the non-linearity of the flux limiter on the solution changes. For $Co = 0.1$, shown in Fig. 11, no undershoots or overshoots form using the SUPERBEE scheme and the final solution at $t = 1.5$ s is oscillation-free. On the other hand, increasing the time-step to a corresponding Courant number of $Co = 0.5$ or $Co = 0.7$, the magnitude of the undershoots and overshoots increases substantially, as observed in Fig. 11 for $t = 0.1$ s, compared to the results obtained for $Co = 0.3$, shown in Fig. 10. For $Co = 0.5$ and $Co = 0.7$ the oscillations of the final solution at $t = 1.5$ s reach an amplitude of $> 10^6$. This behaviour is expected since the non-linearity and the related errors in the evaluation of the flux limiter are a function of the change in solution over one time increment.

5.4. Extrapolation of the upwind node

The extrapolation of the upwind value required for TVD differencing is a particular hurdle for the application on unstructured meshes. As discussed in Section 3.2, two methods to extrapolate the value at the virtual upwind node, using data readily available on unstructured meshes, are considered. Given how the virtual upwind node is incorporated in the gradient ratio r_f , the extrapolation method of Darwish and Moukalled [13] is referred to as *implicit* extrapolation and the method introduced by Ubbink and Issa [12] as *explicit* extrapolation. Both methods precisely reconstruct the upwind value for equidistant, rectilinear meshes but fail to do so on non-equidistant or non-rectilinear meshes, as discussed in Section 3.2. Using the explicit extrapolation method this issue can be rectified by imposing appropriate limits on the extrapolated upwind value.

Fig. 12 shows that a small undershoot can be observed for the solution of the tangential step advection on the tetrahedral mesh, obtained with the SUPERBEE scheme and applying the implicit extrapolation of the upwind value. This oscillation is absent in the solutions obtained with the MINMOD or the van Leer schemes for either extrapolation method as well as with the SUPERBEE scheme when the upwind value is extrapolated and bounded using the explicit method of Ubbink and Issa [12]. Figs. 13 and 14 examine the implicit extrapolation method for the normal step advection on the tetrahedral mesh using the considered TVD schemes. The solution develops particularly large oscillations with the SUPERBEE scheme, shown in Fig. 13, with visible undershoots and overshoots after only one time-step. Evidently, these oscillations originate at the

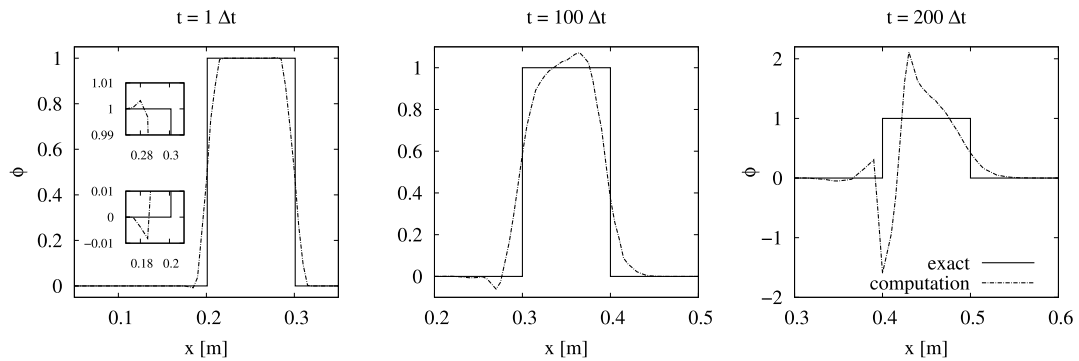


Fig. 13. Temporal evolution of oscillations in the solution along the x -axis for the normal step advection on the tetrahedral mesh, using the implicit upwind extrapolation of Darwish and Moukalled [13] in conjunction with the SUPERBEE scheme.

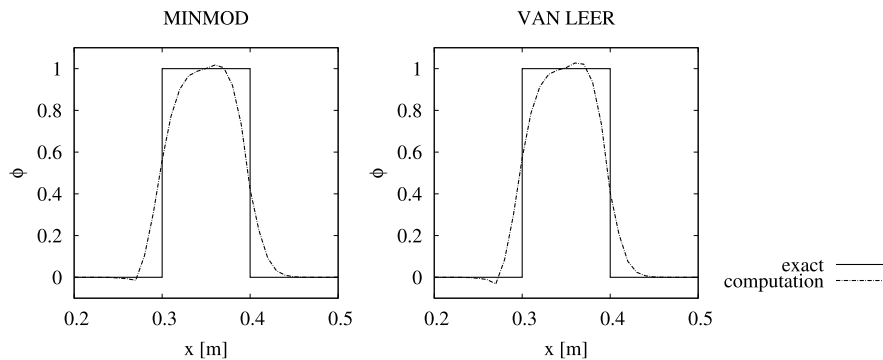


Fig. 14. Profile of ϕ along the x -axis of the normal step advection on the tetrahedral mesh after $t = 100 \Delta t = 0.1$ s using the implicit upwind extrapolation of Darwish and Moukalled [13] in conjunction with the MINMOD scheme and the van Leer scheme.

upwind-side of the discontinuities. Similar as for the oscillations as a result of non-linearity discussed in the previous section, the upwind-side is more sensitive to inaccuracies in the computation of the gradient ratio than the downwind-side, especially with respect to the SUPERBEE scheme. The results obtained with the MINMOD and van Leer schemes, shown in Fig. 14, display similar oscillations, albeit with smaller amplitude, as observed using the SUPERBEE scheme. Extrapolating and bounding the virtual upwind value explicitly, however, results in an oscillation-free solution of the normal step advection on the tetrahedral mesh for all considered TVD schemes, as seen in Fig. 9.

5.5. Correction of mesh skewness

The method to correct the diffusion-like error introduced by mesh skewness, as proposed in Section 4, is tested by means of the three considered test-cases on tetrahedral meshes. The first-order TVD limits (FOL) and second-order TVD limits (SOL), as discussed in Section 4.2, are evaluated separately to examine their impact and performance individually.

Examining the tangential step advection, the skewness-correction provides a visible improvement for the MINMOD scheme and the van Leer scheme, but fails to make a sizeable impact for the SUPERBEE scheme, as shown in Fig. 15. In fact, the SOL-correction increases the diffusiveness of the SUPERBEE scheme noticeably. A similar behaviour can be observed for the normal wave advection, shown in Fig. 16, where the skewness-correction provides a clear improvement for the MINMOD and van Leer schemes, being able to retain the sinusoidal profile of the scalar field almost exactly. For both the MINMOD and the van Leer scheme a visible difference between the FOL and SOL can be identified, with FOL providing a higher accuracy. The impact of the skewness-correction and the choice of TVD limits becomes most pronounced for the normal step advection, shown in Fig. 17. Applying the proposed skewness-correction significantly improves the representation of the double-step profile for the considered TVD schemes. Furthermore, a profound difference between FOL and SOL is observed. The SOL-correction is not able to further improve the result obtained with the SUPERBEE scheme compared to the result obtained with the original, uncorrected SUPERBEE scheme.

Interestingly, although the SUPERBEE scheme is theoretically the best suited second-order TVD scheme for the advection of a step profile due to its compressiveness, as for instance observed in Figs. 7 and 9, the SUPERBEE scheme does not perform well in conjunction with the proposed skewness-correction, contrary to the behaviour of the MINMOD and van Leer schemes. This behaviour can be attributed to the TVD limits imposed on the skewness-corrected flux limiter. Applying SOL, the flux limiter of the SUPERBEE scheme can only be adjusted in the diffusive direction, since the SUPERBEE scheme is

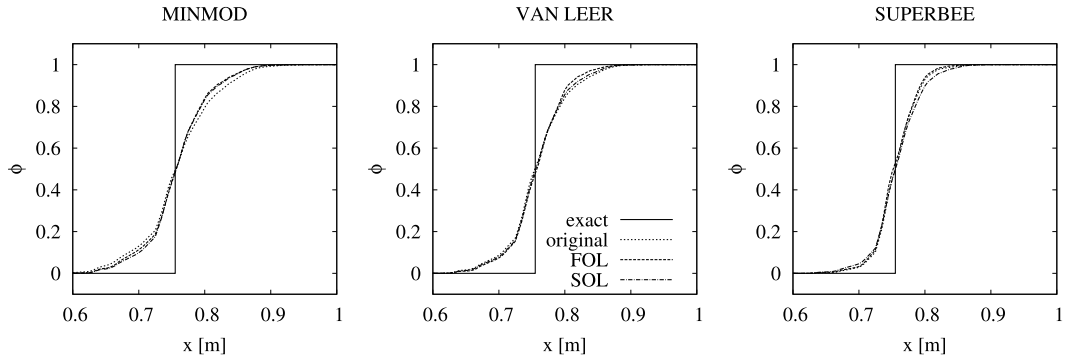


Fig. 15. Profile of ϕ along the x -axis at $y = 0.9$ m of the tangential step advection on the tetrahedral mesh, applying the explicit upwind extrapolation and bounding of Ubbink and Issa [12] without correction of mesh skewness (original) and with correction of mesh skewness, applying first-order (FOL) and second-order (SOL) TVD limits.

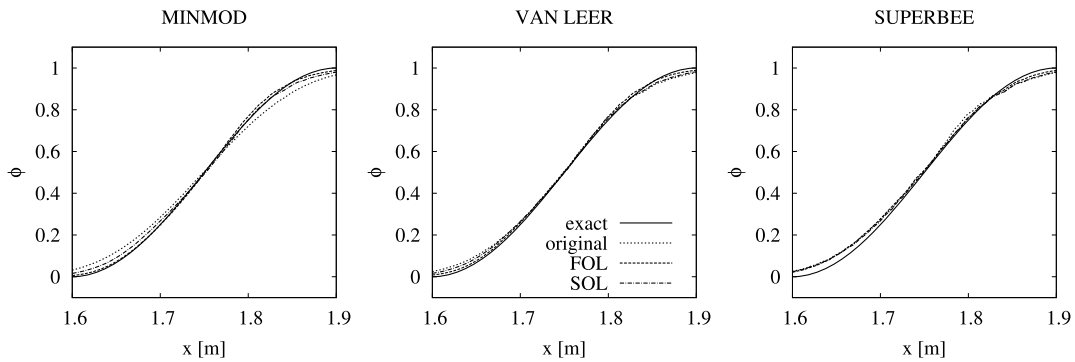


Fig. 16. Profile of ϕ along the x -axis at $t = 1.5$ s of the normal wave advection on the tetrahedral mesh, applying the explicit upwind extrapolation and bounding of Ubbink and Issa [12] without correction of mesh skewness (original) and with correction of mesh skewness, applying first-order (FOL) and second-order (SOL) TVD limits.

already following the compressive limit of the second-order TVD region. A similar problem arises for the MINMOD scheme which follows the diffusive limit of the second-order TVD region and, hence, the skewness-correction with SOL can adjust the flux limiter only in the compressive direction. However, for the presented test-cases this limitation of the MINMOD scheme has evidently no sizeable influence on the performance of the SOL-correction, indicating that adjusting the flux limiter in the compressive direction is more important for the efficacy of the skewness-correction than the correction in the diffusive direction. For all three tested TVD schemes the skewness-correction with FOL provides more accurate results than with SOL. On first view this might be surprising, given the higher formal order of accuracy of the SOL. However, the increase in accuracy of FOL compared to SOL is the result of the larger parameter space available to adjust the flux limiter, as seen in Fig. 3. This is particularly important for mesh faces with sizeable skewness and in regions with large gradients of the advected scalar, such as in the case of the discontinuous double-step profile of the normal step advection case.

Directly comparing the results of the normal step advection obtained with the FOL-correction for the considered TVD schemes, as shown in Fig. 18, reveals that the van Leer scheme provides the most accurate result, closely followed by the MINMOD scheme. Both schemes allow the skewness-correction to adjust the flux limiter over a wide range, in the diffusive as well as the compressive direction, for all gradient ratios $r_f > 0$. The SUPERBEE scheme, on the other hand, follows the compressive limit for $0 \leq r_f \leq 1/L$ and $r_f \geq L$, which constraints the efficacy of the skewness-correction. A similar observation with respect to the relation between the ability to adjust the flux limiter in the diffusive and the compressive direction and the efficacy and robustness of skewness-corrections has been reported in the context of the advection of sharp interfaces by Denner and van Wachem [21].

6. Conclusions

In this article the implementation and performance of TVD schemes on three-dimensional unstructured meshes has been studied and a novel monotonicity-preserving skewness correction for TVD schemes has been proposed. The presented numerical analysis highlights important difficulties of the application of TVD schemes in general and on unstructured meshes in particular.

Accounting for the non-linearity inherently introduced by the evaluation of the TVD flux limiter is critical to assure a monotonicity-preserving implementation and an oscillation-free solution, especially for very compressive TVD schemes, such

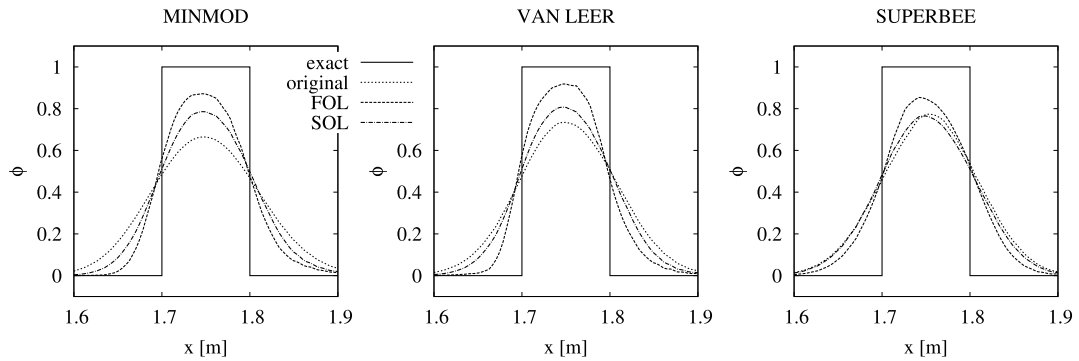


Fig. 17. Profile of ϕ along the x -axis at $t = 1.5$ s of the normal step advection on the tetrahedral mesh, applying the explicit upwind extrapolation and bounding of Ubbink and Issa [12] without correction of mesh skewness (original) and with correction of mesh skewness, applying first-order (FOL) and second-order (SOL) TVD limits.

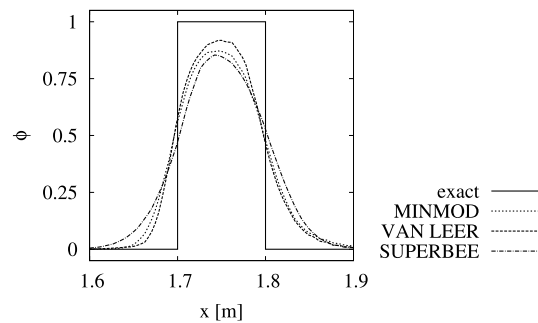


Fig. 18. Direct comparison of the solutions along the x -axis at $t = 1.5$ s of the normal step advection on the tetrahedral mesh using the explicit upwind extrapolation and bounding of Ubbink and Issa [12] and the correction of mesh skewness with first-order TVD limits (FOL).

as the SUPERBEE scheme, as well as in cases with large gradients of the advected variable, e.g. shocks, and large Courant numbers. An iterative solution method to account for the non-linearity (inexact Newton method) has been demonstrated in this study to be an effective way to account for the non-linearity of TVD differencing.

A central problem for the implementation of TVD schemes on arbitrary, unstructured meshes is the determination of the value at the upwind node, which is not readily available. Extrapolation methods proposed by Ubbink and Issa [12] and Darwish and Moukalled [13] are able to reconstruct this upwind value on equidistant, rectilinear meshes, yet fail to provide an accurate upwind value on non-equidistant or, generally, on unstructured meshes, which can lead to an oscillatory solution. Explicitly bounding the extrapolated upwind value based on the values in the vicinity of the upwind node has been shown in this article to be an effective remedy of this problem and assures an oscillation-free solution.

The numerical experiments presented and discussed in this article demonstrate the efficacy and robustness of the newly proposed correction method in diminishing numerical diffusion resulting from mesh skewness on unstructured meshes. The novel skewness-correction method is particularly effective for TVD schemes which do not follow the diffusive or compressive bounds of the second-order TVD region, such as the van Leer scheme, where a correction of the flux limiter toward the upwind (diffusive) and downwind (compressive) values is possible without violating the imposed limits of the flux limiter. Furthermore, the presented skewness-correction does not affect the conservation properties and monotonicity-preservation of the underlying TVD scheme. Interestingly, bounding the skewness-corrected flux limiter within the first-order TVD limits provides a higher absolute accuracy than bounding the flux limiter within the second-order TVD limits, leading to smaller total errors despite the lower formal order of accuracy.

Based on the presented results, the van Leer scheme is the best choice of the considered TVD schemes for unstructured meshes, in particular in conjunction with the proposed correction of mesh skewness. A similar trend, in which the van Leer scheme performs better than other TVD schemes on unstructured meshes compared to the relative performance on structured meshes can be observed in results reported by Li et al. [8] and Hou et al. [9,10]. The van Leer scheme performs consistently well in the considered cases since it is able to represent smooth as well as discontinuous variations with sufficient accuracy and without distorting the solution. The van Leer scheme also provides the opportunity to correct the flux limiter in both directions, diffusive and compressive, in order to account for errors due to mesh skewness.

Acknowledgement

The authors are grateful to the Engineering and Physical Sciences Research Council (EPSRC) for their financial support (grant EP/K008595/1). Data supporting this publication can be obtained from <http://dx.doi.org/10.5281/zenodo.18889> under a Creative Common Attribution license.

References

- [1] J. Ferziger, M. Perić, *Computational Methods for Fluid Dynamics*, 3rd ed., Springer-Verlag, Berlin, Heidelberg, New York, 2002.
- [2] R. LeVeque, *Finite Volume Methods for Hyperbolic Problems*, Cambridge University Press, 2002.
- [3] H.K. Versteeg, W. Malalasekera, *An Introduction to Computational Fluid Dynamics: The Finite Volume Method*, 2nd ed., Pearson Education, 2007.
- [4] S. Patankar, *Numerical Heat Transfer and Fluid Flow*, Hemisphere Publishing Company, 1980.
- [5] A. Harten, High resolution schemes for hyperbolic conservation laws, *J. Comput. Phys.* 49 (1983) 357–393.
- [6] P. Sweby, High resolution schemes using flux limiters for hyperbolic conservation laws, *SIAM J. Numer. Anal.* 21 (1984) 995–1011.
- [7] C. Hirsch, *Numerical Computation of Internal and External Flows, Computational Methods for Inviscid and Viscous Flows*, vol. 2, Wiley, 1990.
- [8] L.-x. Li, H.-s. Liao, L.-j. Qi, An improved r-factor algorithm for TVD schemes, *Int. J. Heat Mass Transf.* 51 (2008) 610–617.
- [9] J. Hou, F. Simons, R. Hinkelmann, Improved total variation diminishing schemes for advection simulation on arbitrary grids, *Int. J. Numer. Methods Fluids* 70 (2012) 359–382.
- [10] J. Hou, F. Simons, R. Hinkelmann, A new TVD method for advection simulation on 2D unstructured grids, *Int. J. Numer. Methods Fluids* 71 (2013) 1260–1281.
- [11] S. Bidadi, S. Rani, Quantification of numerical diffusivity due to TVD schemes in the advection equation, *J. Comput. Phys.* 261 (2014) 65–82.
- [12] O. Ubbink, R. Issa, A method for capturing sharp fluid interfaces on arbitrary meshes, *J. Comput. Phys.* 153 (1999) 26–50.
- [13] M. Darwish, F. Moukalled, TVD schemes for unstructured grids, *Int. J. Heat Mass Transf.* 46 (2003) 599–611.
- [14] H. Jasak, H. Weller, A.D. Gosman, High resolution NVD differencing scheme for arbitrarily unstructured meshes, *Int. J. Numer. Methods Fluids* 31 (1999) 431–449.
- [15] D. Zhang, C. Jiang, C. Yang, Y. Yang, Assessment of different reconstruction techniques for implementing the NVSF schemes on unstructured meshes, *Int. J. Numer. Methods Fluids* 74 (2014) 189–221.
- [16] H. Jasak, Error analysis and estimation for the finite volume method with applications to fluid flow, Ph.D. thesis, Imperial College London, 1996.
- [17] F. Juretić, A.D. Gosman, Error analysis of the finite-volume method with respect to mesh type, *Numer. Heat Transf., Part B, Fundam.* 57 (2010) 414–439.
- [18] F. Denner, B.G.M. van Wachem, Fully-coupled balanced-force VOF framework for arbitrary meshes with least-squares curvature evaluation from volume fractions, *Numer. Heat Transf., Part B, Fundam.* 65 (2014) 218–255.
- [19] I. Demirdžić, S. Muzaferija, Numerical method for coupled fluid flow, heat transfer and stress analysis using unstructured moving meshes with cells of arbitrary topology, *Comput. Methods Appl. Mech. Eng.* 125 (1995) 235–255.
- [20] S. Karimian, A. Straatman, Discretization and parallel performance of an unstructured finite volume Navier–Stokes solver, *Int. J. Numer. Methods Fluids* 52 (2006) 591–615.
- [21] F. Denner, B.G.M. van Wachem, Compressive VOF method with skewness correction to capture sharp interfaces on arbitrary meshes, *J. Comput. Phys.* 279 (2014) 127–144.
- [22] M. Darwish, F. Moukalled, Convective schemes for capturing interfaces of free-surface flows on unstructured grids, *Numer. Heat Transf., Part B, Fundam.* 49 (2006) 19–42.
- [23] S. Balay, J. Brown, K. Buschelman, V. Eijkhout, W. Gropp, D. Kaushik, M. Knepley, L. McInnes, B. Smith, H. Zhang, *PETSc users manual*, 2011.
- [24] S. Balay, W. Gropp, L.C. McInnes, B.F. Smith, Efficient management of parallelism in object oriented numerical software libraries, in: E. Arge, A. Bruaset, H. Langtangen (Eds.), *Modern Software Tools in Scientific Computing*, Birkhäuser Press, 1997, pp. 163–202.
- [25] R. Dembo, S. Eisenstat, T. Steihaug, Inexact Newton methods, *SIAM J. Numer. Anal.* 19 (1982) 400–408.
- [26] P. Wesseling, *Principles of Computational Fluid Dynamics*, Springer, 2001.
- [27] B. van Leer, Towards the ultimate conservative difference scheme. II. Monotonicity and conservation combined second-order scheme, *J. Comput. Phys.* 14 (1974) 361–370.
- [28] S. Osher, S. Chakravarthy, High resolution schemes and the entropy condition, *SIAM J. Numer. Anal.* 21 (1984) 955–984.
- [29] P. Roe, Characteristic-based schemes for the Euler equations, *Annu. Rev. Fluid Mech.* 18 (1986) 337–365.
- [30] B.P. Leonard, The ULTIMATE conservative difference scheme applied to unsteady one-dimensional advection, *Comput. Methods Appl. Mech. Eng.* 88 (1991) 17–74.
- [31] P. Zwart, G. Raithby, M. Raw, An integrated space–time finite-volume method for moving-boundary problems, *Numer. Heat Transf., Part B, Fundam.* 34 (1998) 257–270.